Interannual teleconnections between the summer North Atlantic Oscillation and the East Asian summer monsoon

Hans W. Linderholm,[1] Tinghai Ou,[1,2] Jee-Hoon Jeong,[1] Chris K. Folland,[3] Daoyi Gong,[4] Hongbin Liu,[5] Yu Liu,[6] and Deliang Chen[1]

Received 22 October 2010; revised 23 February 2011; accepted 6 April 2011; published 13 July 2011.

[1] Here we present a study of the relationship between July–August (JA) mean climate over China, which is strongly linked to the East Asian summer monsoon (EASM), and the summer (JA) North Atlantic Oscillation (SNAO). The variations of temperature, precipitation, and cloud cover related to the SNAO were analyzed for the period 1951–2002 using gridded data sets as well as instrumental data from 160 stations in China. It was shown that the major patterns of summer climate over China are highly connected with the interannual variation of the SNAO, supporting a teleconnection between the North Atlantic region and East Asia. Based on the analyses of the daily and monthly reanalysis data sets, we propose possible mechanisms of this teleconnection. Changes in the position of the North Atlantic storm tracks and transient eddy activity associated with the positive (negative) SNAO phase contribute downstream to negative (positive) sea level pressure anomalies in northeastern East Asia. In negative SNAO years, a stationary wave pattern is excited from the southern SNAO center over northwestern Europe to northeastern East Asia. However, during positive SNAO years, a stationary wave pattern is excited extending from the SNAO center across the central Eurasian continent at around 40°N and downstream to the southeast. This may explain a connection between the positive SNAO and atmospheric circulation in middle and southeastern China.

Citation: Linderholm, H. W., T. Ou, J.-H. Jeong, C. K. Folland, D. Gong, H. Liu, Y. Liu, and D. Chen (2011), Interannual teleconnections between the summer North Atlantic Oscillation and the East Asian summer monsoon, *J. Geophys. Res.*, *116*, D13107, doi:10.1029/2010JD015235.

1. Introduction

[2] The summer climate of China, especially in the east, is largely controlled by the East Asia summer monsoon (EASM). A large part of the annual precipitation falls during summer, exhibiting large interannual and interdecadal variations. Summer precipitation over northern and western China is mainly associated with the westerlies. In eastern China, summer precipitation is largely influenced by water vapor transport from the Bay of Bengal, the South China Sea and the western Pacific Ocean, associated with the movement of the EASM [*Ninomiya and Kobayashi*, 1999; *Ding and Hu*, 2003; *Zhou and Yu*, 2005]. In addition, the location and shape of the West Pacific Subtropical High ridge (WPSH) which extends toward eastern China influences the movement of the summer rainfall belt and associated rainfall patterns [*Sha and Guo*, 1998; *Gong and He*, 2002; *Wu et al.*, 2003]. Recently, there has been an increasing trend of summer precipitation over the mid–lower reaches of the Yangtze River around 30°N and a decreasing trend to the north over the Yellow River basin near 38°N [*Ren et al.*, 2000; *Zhang et al.*, 2009]. Consequently, in the last two decades, north and northeastern China have suffered from severe and persistent droughts, while the Yangtze River basin and southern China have been subjected to heavy rainfall and flood events [*Ding et al.*, 2008]. These trends have been associated with a weakening of the EASM since the 1960s [e.g., *Zhou et al.*, 2009, Figure 1]. Moreover, a summer warming trend has been seen over much of China, mainly associated with increases in daily minimum temperatures [*Wang and Gong*, 2000; *Wang and Gaffen*, 2001]. However, in the Sichuan Basin and parts of central and eastern China, a significant cooling trend in summer temperatures has been observed, mainly due to decreasing daily maximum temperatures [*Qian et al.*, 1996; *Qian and Giorgi*, 1999].

[3] The EASM is one of the distinct components of the Asian summer monsoon system influencing weather and climate over eastern Asia, as well as on a global scale [*Ding*,

[1]Regional Climate Group, Department of Earth Sciences, University of Gothenburg, Gothenburg, Sweden.
[2]School of Geography, Beijing Normal University, Beijing, China.
[3]Met Office Hadley Centre for Climate Change, Exeter, UK.
[4]State Key Laboratory of Earth Surface Processes and Resource Ecology, Beijing Normal University, Beijing, China.
[5]Laboratory for Climate Studies, National Climate Center, China Meteorological Administration, Beijing, China.
[6]State Key Laboratory of Loess and Quaternary Geology, Institute of Earth Environment, Chinese Academy of Sciences, Xi'an, China.

0148-0227/11/2010JD015235

2004]. The characteristics of the EASM have been thoroughly studied, e.g., its onset, seasonal march, variability and accompanying anomalous climate events, as well as remote teleconnections [*Ding and Chan*, 2005; *Chang et al.*, 2006; *Wang*, 2006, and references therein]. On seasonal to interannual time scales, Asian summer monsoon variability is strongly related to the El Niño–Southern Oscillation (ENSO), variations in preceding winter and spring Eurasian snow cover, tropical sea surface temperatures, and the movement of the intertropical convergence zone [*Yang and Lau*, 1998; *Webster et al.*, 1998; *Robock et al.*, 2003; *Hung et al.*, 2004]. On interdecadal time scales, changes in the tropical Walker and the Hadley circulation [*Wu and Wang*, 2002; *Wang*, 2006], the East Asian westerly Jet stream and the WPSH are known to have significant influences on the EASM [*Gong and Ho*, 2003].

[4] In addition, remote influences of mid-to-high latitude atmospheric and ocean circulation on climate in east central Asia have been explored to some extent. The Atlantic Multidecadal Oscillation (AMO) has been linked to multidecadal variability of climate in the region, mainly through the EASM [*Lu et al.*, 2006; *Goswami et al.*, 2006; *Feng and Hu*, 2008], while SSTs in the tropical Atlantic may directly influence temperature and precipitation [*Wang et al.*, 2009]. On interannual to decadal time scales, atmospheric circulation features, such as the spring Arctic Oscillation (AO) and the winter/spring North Atlantic Oscillation (NAO), have been suggested to have an impact on summer climate in China [*Liu and Yin*, 2001; *Gong and Ho*, 2003; *Yang et al.*, 2004; *Sung et al.*, 2006; *Sun et al.*, 2008]. For example, it was found that the May AO has an influence on year-to-year EASM variability in parts of China; significant negative correlations between May AO and summer precipitation were found in the mid–lower reaches of the Yangtze River [*Gong et al.*, 2002; *Gong and Ho*, 2003]. On interdecadal time scales, summer precipitation variability over China has been related to March NAO [*Gu et al.*, 2009] and May AO [*Gong and Ho*, 2003], although this relationship may not be temporally stable [*Gu et al.*, 2009]. However, despite all these studies, the EASM remains difficult to predict and model [*Zhou et al.*, 2009].

[5] Coming to the focus of this paper, most studies of associations between the NAO and regional to hemispheric climate have been during winter, when the largest amplitude anomalies in mean sea level pressure (MSLP) occur and NAO variability is larger than in other seasons [*Hurrell et al.*, 2003]. However, leading atmospheric circulation patterns broadly similar to the winter NAO are found in other seasons [*Barnston and Livezey*, 1987; *Hurrell and van Loon*, 1997; *Hurrell et al.*, 2003]. Eigenvector (EOF) analysis of the annual cycle in the North Atlantic/Arctic region of seasonal NCEP MSLP anomalies gives a set of seasonally varying dipole patterns including the familiar winter NAO. In summer, the scale of the NAO EOF pattern is smaller such that its southern node stretches from near UK to Scandinavia rather than the Azores – Spain region seen in winter [*Hurrell and Folland*, 2002; *Hurrell et al.*, 2003].

[6] A prime motivation for this paper is the significant pattern of correlations, shown by *Folland et al.* [2009] in their Figure 7, between the SNAO and storm tracks over northern China. Thus, when the SNAO index is in its positive phase, the storm track over the eastern Atlantic and Europe shifts north and extends into western Russia at higher latitudes. With a short break, this enhanced northern storm track then extends over southern Siberia and Mongolia into northern China and toward Korea. The reverse relationship is expected for the negative SNAO index phase. Accordingly, a positive SNAO would be expected to be associated with wetter than normal conditions close to this storm track including China mostly north of Beijing. *Folland et al.* [2009] did not analyze southern China. So in this paper we extend the storm track analyses to all of China and study the spatial relationships between Chinese climate, the SNAO and the associated changes in storm tracks and atmospheric circulation.

2. Data

[7] The SNAO is represented as the principal components time series corresponding to the leading EOF of daily MSLP anomalies from the EMULATE data set [*Ansell et al.*, 2006] over extratropical European–North Atlantic sector (25°N–70°N, 70°W–50°E) for July and August 1881–2003. The leading EOF exhibits the north-south dipole pattern of MSLP over Western Europe to Greenland, which explains about 18% of the daily variance over the analyses domain and 28% of the July–August mean variance [*Folland et al.*, 2009]. An EOF analysis over this domain for 1881–2003 in summer recreates mainly the southern part of the full summer EOF node seen in NCEP data; when the southern node has higher (lower) than average pressure the SNAO index is in a positive (negative) phase. The temporal stability of the SNAO is shown by similar spatial patterns on daily to two month time scales; in addition, regression of the SNAO against 500 hPa and 300 hPa heights gives nearly equivalent barotropic patterns [*Folland et al.*, 2009].

[8] Monthly precipitation and temperature data from 160 stations, relatively evenly distributed over China, were used to study the relation between the SNAO and July–August temperature and precipitation in China. The data were provided and quality controlled by the China Meteorological Administration, covering the period 1951–2002. These data sets have been widely used to study changes and variations of climate in China [*Gemmer et al.*, 2004; *Lu*, 2009; *Zhang et al.*, 2009]. In order to more clearly study the connection between the SNAO and summer climate in China, monthly observed cloud cover data over China were used, where monthly total cloud cover values from the 160 stations was averaged from daily total cloud cover. Most of the stations start their observations of cloud cover in 1951; 52 stations have full cloud cover data for 1951–2002, 70 stations have missing data of cloud cover for less than 5 years and 159 stations have at least 36 years of cloud cover over 1951–2002. In order to illustrate the spatial variation of precipitation anomalies related to the evolution of daily positive/negative SNAO events, a daily gridded precipitation data set for China, interpolated from around 700 stations [*Chen et al.*, 2010], was used.

[9] Global gridded precipitation, temperature and cloud cover data sets were also analyzed to evaluate the influence of the SNAO on summer climate in Eurasia. For temperature, the Climate Research Unit (CRU) 0.5° × 0.5° resolution observed global land temperature data set [*Mitchell and Jones*, 2005] was used. These data have been compared with several observational climate data sets in China with good consistency [*Wen et al.*, 2006]. The CRU global 0.5° × 0.5° resolution cloud cover data set was also used [*Mitchell*

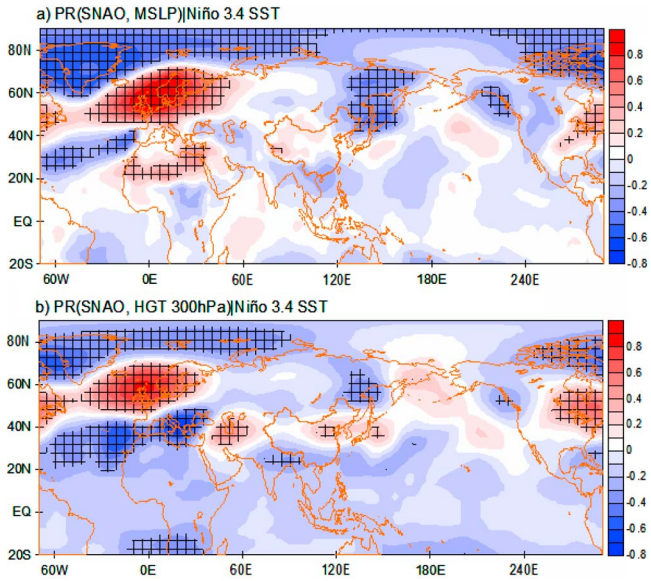

Figure 1. Partial correlations, independent of Niño 3.4 SST, between the summer (July–August) North Atlantic Oscillation (SNAO) and (a) July–August MSLP and (b) July–August 300 hPa HGT 1951–2002. All data were filtered to highlight the interannual variability (see text for details). Positive and negative correlations locally significant at the 5% confidence level are indicated by black crosses here and in other diagrams.

and Jones, 2005]. Other climate variables, such as global land surface precipitation, are also included in the CRU data sets, but in order to compare the influence of the SNAO on precipitation and temperature independently, global 2.5° × 2.5° resolution gauge-based land surface precipitation from the Global Precipitation Climatology Centre (GPCC, http://gpcc.dwd.de) was used. These data are available for 1901–2007, but only data from 1951 to 2002 were used in this study. Detailed information about the GPCC gridded precipitation data set can be found in several publications [*Rudolf et al.*, 1994; *Beck et al.*, 2005; *Rudolf and Rubel*, 2005; *Rudolf and Schneider*, 2005; *Schneider et al.*, 2008].

[10] To examine the Northern Hemisphere circulation changes associated with the SNAO, reanalysis data sets from NCEP/NCAR [*Kistler et al.*, 2001] were utilized. To represent the strength of East Asian Summer (JA) Monsoon, the Wang and Fan index (WFI) defined by *Wang and Fan* [1999] was selected. The WFI is a shear vorticity index, highly correlated with the leading PC of the EASM (r = 0.97), and it does not only represent the leading modes of tropical and subtropical–extratropical rainfall variability well, but also represents extremely well the low-level monsoon wind variability [*Wang et al.*, 2008]. The WF index is defined by the $U850_{(5°–15°N,\ 90°–130°E)}$ minus $U850_{(22.5°–\ 32.5°N,\ 110°–140°E)}$, and physically, the WFI reflects the variations in both the Western North Pacific monsoon trough and subtropical high; the two subsystems which are the key elements of the EASM circulation system [*Wang et al.*, 2008]. The WFI was derived from the NCEP/NCAR reanalysis data.

[11] Because the interannual variability of both the SNAO and the EASM are influenced by the ENSO [*Yang and Lau*, 1998; *Webster et al.*, 1998; *Chang et al.*, 2000; *Folland et al.*, 2009; *Li et al.*, 2010], here we utilize the partial correlation (equation (1)) to show relationships between the SNAO and selected climate parameters which are statistically independent from the ENSO:

$$PR_{XY\cdot Z} = \frac{R_{XY} - R_{XZ}R_{YZ}}{\sqrt{1 - R_{XZ}^2}\sqrt{1 - R_{YZ}^2}} \quad (1)$$

where $PR_{XY\cdot Z}$ indicate the partial correlation coefficient between X (e.g., precipitation) and Y (the SNAO) which is independent of Z (ENSO). R_{XY}, R_{XZ} and R_{YZ} indicate the correlation coefficient between X and Y, X and Z and Y and Z, respectively.

[12] Here the ENSO index is represented by Nino 3.4, the average sea surface temperature anomaly in the region bounded by 5°N to 5°S, from 170°W to 120°W (data from NOAA ERSST V3b [*Xue et al.*, 2003; *Smith et al.*, 2008]). All correlation maps shown below utilize partial correlations with the influence of Nino 3.4 SST removed, because we are interested in teleconnection patterns independent of ENSO.

[13] Correlation significance has been estimated using two-sided *t* tests. Moreover, since our emphasis was on examining the interannual association between the SNAO and climate in China, all correlation analyses were performed on high-pass filtered time series, where, using a Gaussian M-term (M = 9) low-pass filter, the long-term variation of the time series was removed from the original time series highlighting periods of ≤9 years.

3. Results

3.1. SNAO and the Large-Scale Circulation

[14] Partial correlations between the SNAO and July–August (JA) MSLP and 300 hPa geopotential heights (NCEP/NCAR reanalysis data), independent of simultaneous values of Nino 3.4 SST, are shown in Figures 1a and b. Over the land areas of the northern Hemisphere, the SNAO shows significant positive correlations with MSLP over northern/central Europe and western Russia, across much of North Africa, eastern North America, and west central China (mainly the Tibetan plateau). Significant negative correlations over land are found over Greenland, the Canadian Arctic and northwestern North America, easternmost Russia as well as part of northeastern China. When the oceans are considered, significant positive correlations are found over the northeastern part of the North Atlantic Ocean, while negative correlations are found over the Arctic Ocean, the central North Atlantic Ocean and Pacific west coast of North America and the Sea of Okhotsk. The SNAO–300 hPa geopotential height correlation pattern is broadly similar to that of MSLP, although with somewhat lower correlations in places. The most prominent feature is that over the North Atlantic/Arctic region where significant positive correlations are found over eastern North America, extending across the northern North Atlantic into the United Kingdom and Scandinavia, and negative correlations over the Arctic and the central North Atlantic, extending into the Mediterranean region. Less extensive regions with positive correlations are found over the near East, east central China, the northwestern Indian Ocean and northeasternmost Russia. Negative correlations are found along the Pacific west coast of North

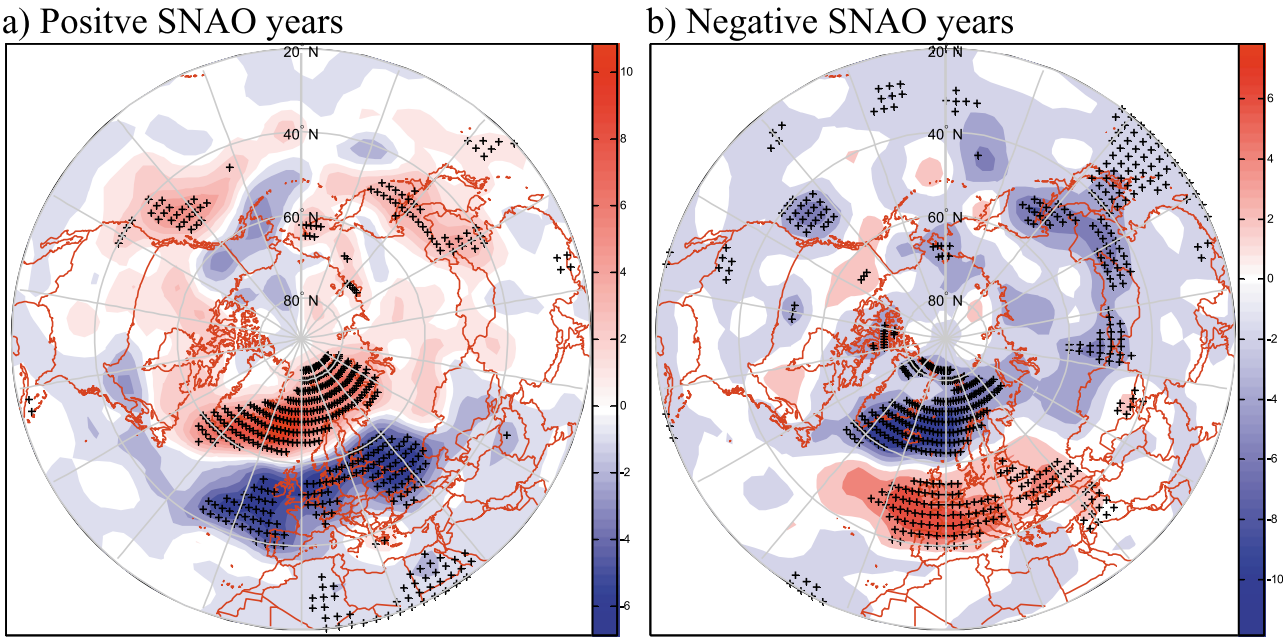

Figure 2. Composite map of 300 hPa storm tracks for (a) positive SNAO years (SNAO index > 1 SD) (1955, 1959, 1968, 1969, 1972, 1975, 1976, 1978, 1981, 1983, 1984, 1990, 1996, 1997, 2002) and (b) negative SNAO years (SNAO index < −1 SD) (1953, 1954, 1956, 1958, 1960, 1965, 1974, 1985, 1988, 1992, 1998) (units: m) (points significant at 10% level are indicated by black crosses). Red indicates increased storm activity, and blue indicates decreased storm activity relative to the average of all data.

America, northeastern India, the Sahel which thus shows a baroclinic structure, and southeastern Russia, extending out over the western Pacific. Summarizing, the pattern of correlations across the hemisphere across the two levels is extremely field significant, with an almost equivalent barotropic structure in mid to high latitudes but with a rather baroclinic structure over some tropical regions.

3.2. SNAO and Storm Tracks

[15] North Atlantic storm tracks show distinct geographical and intensity variations with the phase of the SNAO [*Folland et al.*, 2009]. Composite maps indicating the mean storm tracks for positive and negative SNAO phases are shown in Figure 2. Here storm track activity is estimated from the standard deviation of 300 hPa geopotential height, daily band-pass filtered data on time scales of 2–8 days to highlight regions of strong transient eddy activity. The dipole structure of anomalous storm track activity is clearly seen over the North Atlantic which reverses in sign with SNAO phase. During the negative SNAO phase, a reduction in storm track activity is found over southern Greenland to the Norwegian Sea and Barents Sea, stretching southeastward to Mongolia and northeastern East Asia. Although overall slightly less in magnitude, an increase in storm track activity is found over similar regions in the positive SNAO phase. This pattern is generally consistent with Figure 1, notably for the focus of our analyses over northeastern East Asia. Thus increased (decreased) transient activity appears to be dynamically associated with the negative (positive) MSLP anomalies in the positive (negative) SNAO phase. In addition to transient eddy activity, a possible contribution to the teleconnection patterns in MSLP and geopotential height by stationary wave activity is discussed in section 4.2 below.

3.3. Associations Between SNAO and July–August Precipitation, Temperature, and Cloud Cover

[16] The spatial distribution of the partial correlation coefficients between the SNAO and JA precipitation is shown in Figure 3 for Eurasia and North Africa. As previously shown by *Folland et al.* [2009], a strong region of negative correlation between the SNAO and JA precipitation is found over Northern Europe, with a significant positive correlation between the SNAO and JA precipitation over parts of the Mediterranean and Southern Europe. Additionally, we note the coherent and significant negative correlations throughout the Sahel, much as shown by *Folland et al.* [2009], except that here joint ENSO influences have been removed. Over China, the spatial correlation pattern between the SNAO and GPCC gridded precipitation is quite congruent with the spatial correlation pattern between the SNAO and precipitation data from the 160 instrumental stations. Significant positive correlations occur in southeast China near the coast, while significant negative correlations are located across central eastern China in the region between the Yangtze and Huai Rivers extending west into east Tibet. This spatial pattern of precipitation correlations in East Asia resembles the primary mode of precipitation variation associated with interannual variations of the EASM suggested by *Lau et al.* [2000] and *Wang et al.* [2001]. Moreover, the SNAO and JA precipitation correlation pattern over China is very similar to the first EOF pattern of JA precipitation over China [*Weng et al.*, 1999; *Zhou and Yu*, 2005]. The correlation

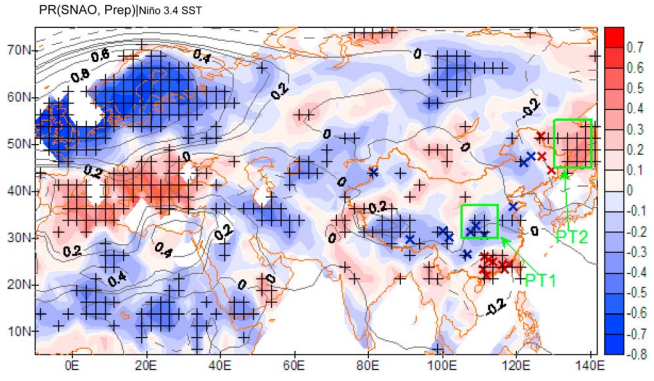

Figure 3. Spatial distribution of the partial correlation coefficients between the SNAO and JA precipitation from the GPCC data set (http://gpcc.dwd.de) and data from 160 stations in China (data from the National Climate Centre) independent of JA Niño 3.4 SST during 1951–2002. Also included are the correlation between SNAO and JA MSLP (contour). Areas with significant correlations (5% level) are indicated by black pluses (GPCC data) and red/blue crosses for the station data. All data were filtered to highlight the interannual variability (see text for details). The two green boxes show two precipitation center regions discussed in the text: PT1: the middle Yangtze River region (30°N–37.5°N, 105°E–115°E); PT2: Northeast China region (45°N–55°N, 130°E–140°E). See the text for more details.

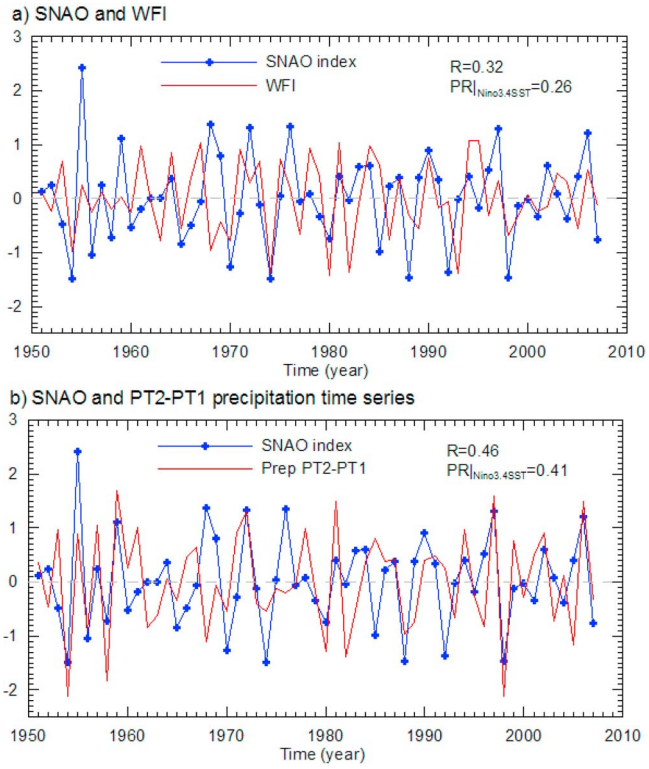

Figure 4. The SNAO index compared to (a) the WFI [*Wang and Fan*, 1999] and (b) the PT2-PT1 precipitation time series (see Figure 3 for locations) during 1951–2007. All data were filtered to highlight the interannual variability (see text for details).

between the SNAO and, the JA WFI [*Wang and Fan*, 1999], was 0.32 for 1951–2007, which is statistically significant at the 5% level (Figure 4a and Table 1). The correlation pattern is also similar to that of the delayed influence of the May AO on Yangtze River summer (JJA) precipitation found by *Gong et al.* [2002] and East Asian summer (JJA) monsoon rainfall [*Gong and Ho*, 2003]. However, while they found that significant May AO–summer precipitation associations were concentrated in the Yangtze River region, Figure 3 shows regions of significant correlation both in the Yangtze River Region and in southeast China.

[17] To highlight the SNAO-related dipole-like structure in precipitation near the coast of East Asia, the difference in precipitation between two regions, PT1 and PT2, was investigated. PT1 is situated in the middle Yangtze River region (30°N–37.5°N, 105°E–115°E) and PT2 is situated in northeast China, extending into Russia (45°N–55°N, 130°E–140°E). The locations of PT1 and PT2 are shown in Figure 3. Figure 4a first shows the relationship between the WFI and the SNAO for 1951–2007; this is only slightly affected by ENSO as the correlation of 0.32 ($p < 0.01$) is only reduced to 0.26 ($p = 0.06$). Positive WFI values indicate a stronger summer monsoon, leading to less precipitation over the Yangtze River basin (PT1) but more precipitation in northeastern China and also in PT2. This would lead to a larger precipitation difference between PT2 and PT1 (PT2-PT1), and is supported by the strong positive correlations between (PT2-PT1) and WFI (Table 1). Moreover, Figure 4b shows that, over the same period, the SNAO is more strongly related to the difference between PT2 and PT1 than to the WFI index, with a correlation of 0.46 which only reduces to 0.41 ($p < 0.01$) when ENSO effects are removed. From Table 1 is evident that the WFI is more strongly related to PT1 than PT2, while the opposite is true for the SNAO.

[18] The spatial distribution of the partial correlation coefficients between the SNAO and JA mean temperatures (Figure 5a) shows similar, but of opposite sign, correlation patterns as those found between the SNAO and precipitation. Again, the correlation patterns obtained using the gridded CRU temperature data set and Chinese station data agree well. Strongly significant positive correlations are found over

Table 1. Correlation Coefficient Between the SNAO Index and JA Mean Precipitation Time Series of Middle Yangtze River Region (PT1: 30°N–37.5°N, 105°E–115°E) and Northeast to China Region (PT2: 45°N–55°N, 130°E–140°E) and an EASM Index (WFI) During 1951–2007[a]

	SNAO	PT1	PT2	PT2-PT1
PT1	−0.34**			
PT2	0.46**	−0.49**		
PT2-PT1	0.46**	−0.87**	0.86**	
WFI[b]	0.32*	−0.53**	0.38**	0.53**

[a]All data were filtered to highlight the interannual variability (see text for details). One asterisk denotes significant at 5% level, and two asterisks denotes significant at 1% level.
[b]WFI from *Wang and Fan* [1999].

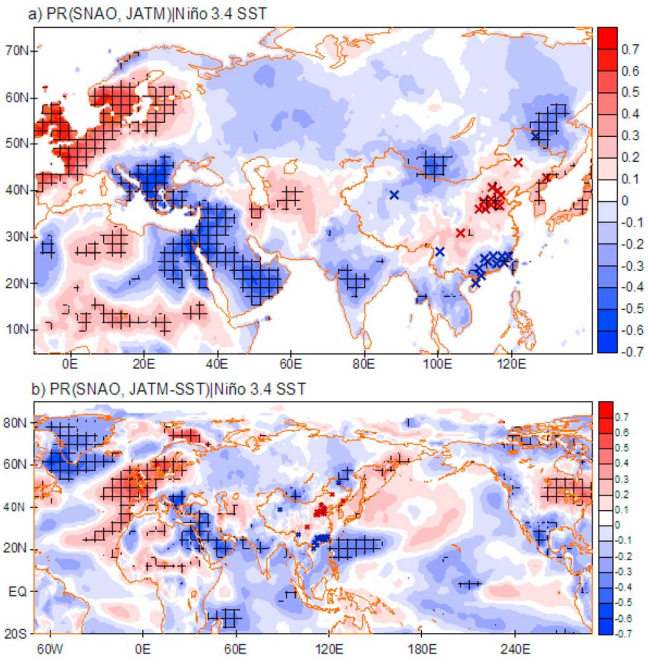

Figure 5. (a) Same as Figure 3 but for partial correlation between the SNAO and JA mean temperatures (CRUTS2.1 and 160 Chinese stations) independent of JA Niño 3.4 SST during 1951–2002. (b) Same as Figure 5a but for larger region and the correlation between SANO and JA mean temperature and NOAA ERSST V3b [*Smith et al.*, 2008; *Xue et al.*, 2003].

northwestern Europe, while the correlations are negative over eastern parts of southern Europe. Over the Sahel, positive correlations are just as widespread and coherent as the negative precipitation correlations. Turning to China, the region of significant negative correlations in southeast China is quite similar to the region of significant positive SNAO-precipitation correlations. But while significant negative correlations between SNAO and JA precipitation were found over central China, a coherent region of significant positive SNAO-temperature correlations is found more to the northeast, west of the Huang Hai (Yellow Sea). Negative correlations are found in northeasternmost China, where also significant negative correlations between SNAO and JA precipitation were found. Regional relationships between precipitation and temperature will depend on both anomalous cloud cover and anomalous advection, the latter mainly away from the tropics, so some differences in the regional detail of rainfall and temperature correlations over China is expected. From Figure 5b it is also clear that the strong ENSO SST signal seen in Figure 4a of *Folland et al.* [2009] has been removed by the partial correlation analyses. The significant negative correlations with SST in the region of the West Pacific Subtropical High corresponds with the MSLP correlation patterns, and in general the correlation patterns between SNAO and SST are consistent with those between SNAO and adjacent land temperatures.

[19] The spatial distribution pattern of the partial correlation between the SNAO and cloud cover is consistent with that of MSLP, temperature and precipitation (Figure 6). Positive correlations are found in southern Europe and North Africa, a belt across central Eurasia, being significant over Kazakhstan and south central Siberia, southeasternmost Russia and southeastern China and further south. Negative correlations occur over northwestern Europe, the Sahel region and along a near-continuous band across southern Eurasia, from the eastern Mediterranean, across the Tibetan Plateau and to northeastern China. Thus we can be confident that most of our key results are real, and not artifacts of particular data sets.

[20] The physically consistency between the precipitation, SAT and cloudiness relationships, and the storm track results of section 3.2, supports a remote relationship between the SNAO and the EASM.

4. Discussion

4.1. Implications for an Association Between SNAO and Chinese Summer Climate

[21] Previous studies have suggested a remote influence of the winter NAO on climate over East Asia through its effects on the Asian jet [*Branstator*, 2002; *Watanabe*, 2004; *Hong et al.*, 2008; *Sung et al.*, 2010]. For instance, *Li et al.* [2008] suggested a teleconnection pattern from the North Atlantic to East Asia, linking climate anomalies of the two regions in late winter (March). In general, previous studies have attempted to establish dynamical links between the NAO in winter and/or spring and summer climate in China, not contemporary or short lead time links in summer. *Sung et al.* [2006] suggested a delayed impact of the winter NAO on East Asian summer monsoon precipitation, where their correlation between December NAO and June precipitation in China and Korea could be related to wave train patterns originating from the North Atlantic. However, they noted a significant change in these relationships around the 1980s. *Gong and Ho* [2003] showed an association between late spring (May) AO and the EASM, where it was proposed that the AO influences surface climate during winter and spring and that the AO-related boundary anomalies impact the atmospheric circulation, and hence the EASM. However, a straightforward mechanism that allows a lag of up to several months for the North Atlantic (or Arctic) signal to reach East Asia has yet to be proposed.

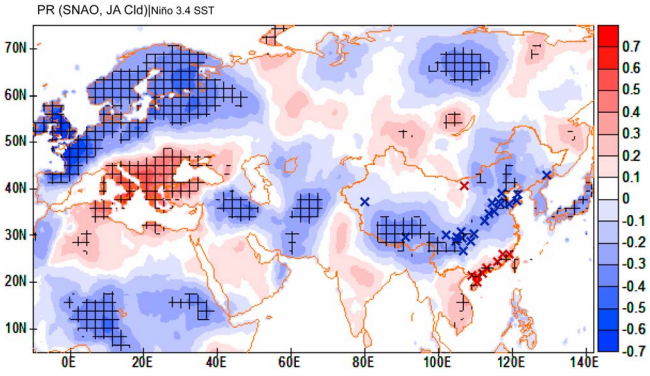

Figure 6. Same as Figure 3 but for partial correlations between the SNAO and JA cloud cover (CRUTS2.1 cloud cover (Cld) and 160 Chinese stations total cloud cover) independent of JA Niño 3.4 SST for 1951–2002.

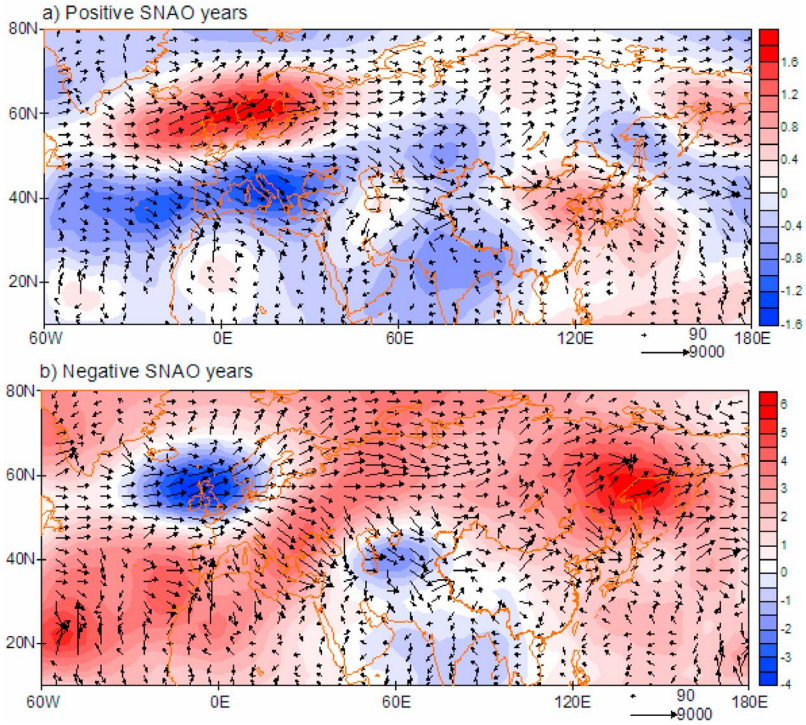

Figure 7. The 300 hPa JA mean wave activity flux (arrow, units: $m^2\ s^{-2}$) and stream function anomaly (units: $10^6\ m^2\ s^{-1}$) for (a) positive and (b) negative SNAO years during 1951–2002. Scaling for the arrows is given near the lower right corner. The propagation of stationary Rossby waves was estimated by the wave activity flux suggested by *Takaya and Nakamura* [1997], which is a generalization of *Plumb*'s [1985] three-dimensional wave activity flux (W) applying to a zonally uniform basic flow. The detailed formulation of W is available from *Takaya and Nakamura* [1997, 2001].

[22] As seen in Figures 3–6, generally consistent variations are found in cloud cover, surface temperature, and precipitation variation with respect to the storm track and MSLP changes, particularly over mid to northeastern China. Thus, our results suggest a consistent link between different measures of atmospheric circulation and climate in East Asia during summer when the SNAO index from *Folland et al.* [2009] is utilized as the common influencing factor. In regions where the SNAO is positively (negatively) correlated with MSLP, negative (positive) correlations to precipitation are found. Thus, when the SNAO index is positive, negative MSLP anomalies are found in southeastern and northeastern China and southeastern Russia coinciding with positive precipitation anomalies. In western China (e.g., the Tibetan Plateau) and in Yangtze River basin positive SNAO anomalies correspond to negative precipitation anomalies. This finding is similar to that of *Liu and Yin* [2001], who linked interannual precipitation variability over the Eastern Tibetan Plateau (ETP) to the upstream zonal flow associated with the summer (June–August) NAO (based on 700 hPa geopotential from *Barnston and Livezey* [1987]). However, a south/north discrepancy in precipitation anomalies at the Eastern Tibetan Plateau, where low (high) NAO index values, summer precipitation yields above (below) normal in the southern ETP but below (above) normal in the northern ETP found by *Liu and Yin* [2001], could not be clearly seen in our results. The significant negative correlation between the SNAO and 300 hPa geopotential heights in northeast China and west of the Yellow River basin may explain the significant negative correlation between the SNAO and JA temperature in these regions. A similar pattern was found by *Gong et al.* [2001], where positive temperature anomalies in northern China coincided with positive 500 hPa geopotential height anomalies, and vice versa. Thus, a teleconnection pattern similar to the "North Atlantic–Ural–East Asia" (NAULEA) pattern in March [*Li et al.*, 2008] seems to link the North Atlantic region and East Asia in summer as well.

4.2. Possible Mechanisms for the Observed Teleconnection

[23] *Folland et al.* [2009] indicated that the SNAO signal has a remote East Asian influence though they did not comment on this. Our analyses indicate that such a teleconnection is partly contributed by storm track changes associated with the SNAO. During positive SNAO years, the North Atlantic storm track moves northward, and more storms (i.e., transient eddies) pass over Iceland to the Norwegian Sea. The pattern of enhanced storm activity is further elongated eastward and southeastward, and the southeastward branch further extends to the eastern part of Eurasian continent through Mongolia where a significant increase of storm activity is also observed compared to negative SNAO years (Figure 2). This seems to indicate an increased propagation of tropospheric eddy activity downstream of the positive relative to the negative

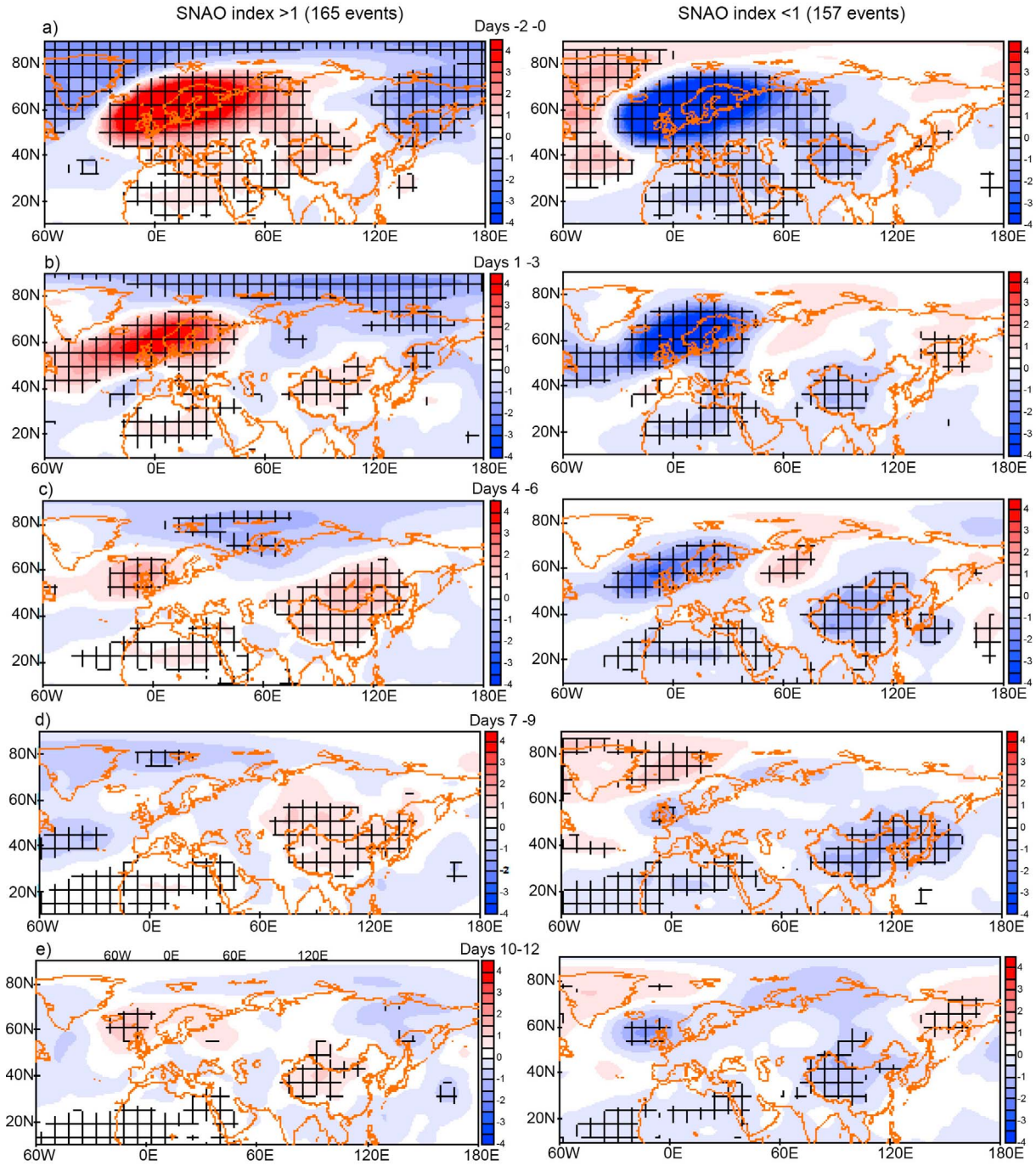

Figure 8. Composite map of 3 day averaged MSLP anomalies (units: hPa) (after removal of the seasonal MSLP cycle), associated with (left) positive and (right) negative SNAO maximum/minimum events (see text for details). Day −2 = two days before a SNAO event, day −1 = one day before an event, day 0 = the day of the event, and so on (points with 5% significance are indicated by crosses). (a) Days −2–0, (b) days 1–3, (c) days 4–6, (d) days 7–9, and (e) days 10–12.

SNAO. Such eddies may be amplified when reaching the eastern coast of the Eurasian continent, where the atmospheric conditions are quite unstable and large amounts of moisture are available in summer. This could result in a significant decrease of MSLP and a related increase in precipitation in coastal northeastern Eurasia in positive SNAO years. During negative SNAO years, on the contrary, the North Atlantic storm track moves southward, and more storms pass through western Europe to southeastern Europe. Transient eddy activities downstream are suppressed at this lower latitude. The weakening of the higher latitude storm track over northern Europe also weakens that passing through the northern Eurasian continent to northeastern Asia. This is consistent with the MSLP change in Figure 1a.

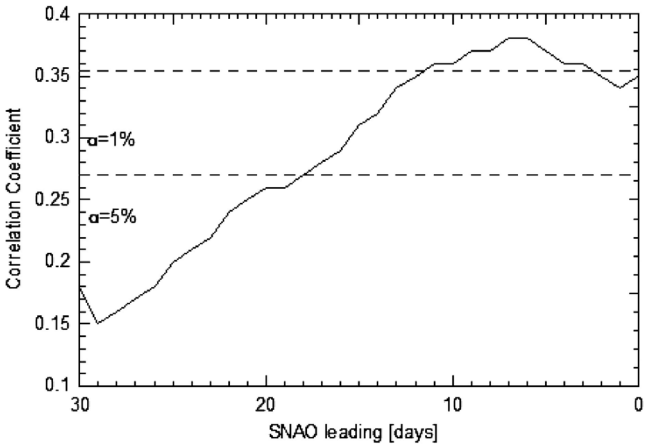

Figure 9. Lagged correlation between the 62 day running average of the SNAO index and JA mean daily precipitation difference between regions PT2 and PT1 (see Figure 3 for locations of the regions) with SNAO leading the precipitation. SNAO index ≥ 1 (165 events) SNAO index ≤ −1 (157 events).

[24] In addition to changes in transient eddy activity, a remote influence of the SNAO may also occur through a stationary wave excited from near the SNAO center. For the winter NAO, *Sung et al.* [2010] have shown that there is a distinct downstream development of circulation anomalies induced by quasi-stationary wave propagation from the NAO center, which affects the Siberian High intensity and temperature in East Asia. We now investigate this idea for the SNAO. Figure 7 shows the quasi stationary wave activity flux phases at 300 hPa, calculated using the method of *Takaya and Nakamura* [1997, 2001], together with 300 hPa stream function anomalies during positive and negative phases of the SNAO. From Figure 7 the wave source region, the direction of propagation, and circulation responses in the upper troposphere measured by stream function anomalies are displayed. While the effect of changes in the transient eddies on MSLP seen in Figure 2 is mainly found in the northeastern part of the Eurasian continent, the quasi stationary wave pattern emanating from the SNAO center seems to explain the MSLP change in the southeastern part of Asia as well. A dominant feature of both phases of the SNAO is a stationary wave emanating from the SNAO center pointing southeastward toward the eastern part of Eurasian continent. The spatial patterns of anomalous stream functions show a quite asymmetric feature with respect to the SNAO phases in association with the wave activity flux. During the positive phase of SNAO, a distinct stationary wave pattern is found over the central Eurasian continent around 40°N, the wave activity flux vectors pointing eastward to East Asia from the southeastern Europe. This pattern appears to be congruent with the anticyclonic circulation anomalies in the positive phase of the SNAO over the mid-China seen in Figure 1a. Furthermore, this pattern (Figure 7a) yields cyclonic circulation anomalies over northern India, which may explain the significant negative correlation between the SNAO and the South Asian Monsoon index (RM1, 10°N–30°N, 70°E–110°E [*Lau et al.*, 2000], not shown) of −0.35. During its negative phase (Figure 7b), the stationary wave extending from the SNAO region is more distinct over the northern part of the Eurasian continent. Here the wave activity flux vectors point directly eastward toward northeastern Eurasia from the northern part of the North Atlantic Ocean. This pattern seems to be consistent with the negative correlation of 300 hPa geopotential height over the northeastern Eurasia and the SNAO seen in Figure 1b.

[25] We also examine composite teleconnection patterns that are explained by the quasi-stationary wave idea in 3 day composites of daily MSLP for each phase of the SNAO index. The 3 day composites were calculated for five periods from just before the given SNAO phase was observed to 10–12 days after its inception and for all days in JA over the period (Figure 8). The maximum and minimum of the daily SNAO index (i.e., day 0) was defined as the day with a SNAO index stronger (weaker) than the previous day (−1) and the following day (+1) when the daily SNAO index was stronger (weaker) than +1(−1). During the development of maximum SNAO events (daily SNAO index ≥ 1; 165 events, from day −2 to day 0, where day 0 is the actual SNAO maximum), a clear positive MSLP pattern is observed over the Atlantic and western European region, while negative MSLP anomalies are found over Northeastern Asia. The spatial pattern of MSLP during the initiation of minimum SNAO events (daily SNAO index ≤ −1; 157 events) is opposite to that of the positive SNAO. This pattern is similar to the spatial pattern of correlation between SNAO and JA MSLP in Figure 1a. The evolution of the composite pattern reflects the characteristics of a quasi-stationary wave. The anomalous *pattern* of MSLP anomalies in the SNAO center and East Asia remains largely constant with time but the *amplitude* of anomalies changes. In the SNAO center, the positive and negative MSLP anomalies of large amplitude are damped with time but the anomalies in East Asia become stronger until days 7–9, and then start to decline. This suggests that the energy associated with the large-scale perturbation in the SNAO center is progressively transferred to East Asia in just over a week.

[26] Given the relatively strong relationship between the SNAO and precipitation in the PT1 and PT2 regions (Figure 3), a similar lag in precipitation following the initiation of an SNAO event is expected. Averaged over JA (62 days), normalized daily SNAO index values based on the climatological period 1880–2003 (as in work by *Folland et al.* [2009]) were correlated against daily mean JA precipitation differences for PT2-PT1 (Figure 9). Here the precipitation data were fixed while the SNAO index was progressively changed to earlier and earlier lead times one day at a time for a total of one month (31 days). The correlation is quite strongly positive at 0.35, ($p < 0.05$), even for simultaneous data, consistent with Figure 3, increasing to near 0.4 ($p < 0.01$) when the maximum positive correlation is obtained for a lead of the SNAO by 7–9 days. This is also consistent with the MSLP composite (Figure 8) in that the maximum MSLP anomalies associated with the SNAO are found 7–9 days after the SNAO maximum/minimum. Figure 10 shows similar results to Figure 8 but for daily precipitation anomalies distributed over the whole of China, using precipitation data from both the gridded interpolated daily precipitation data set [*Chen et al.*, 2010] and from

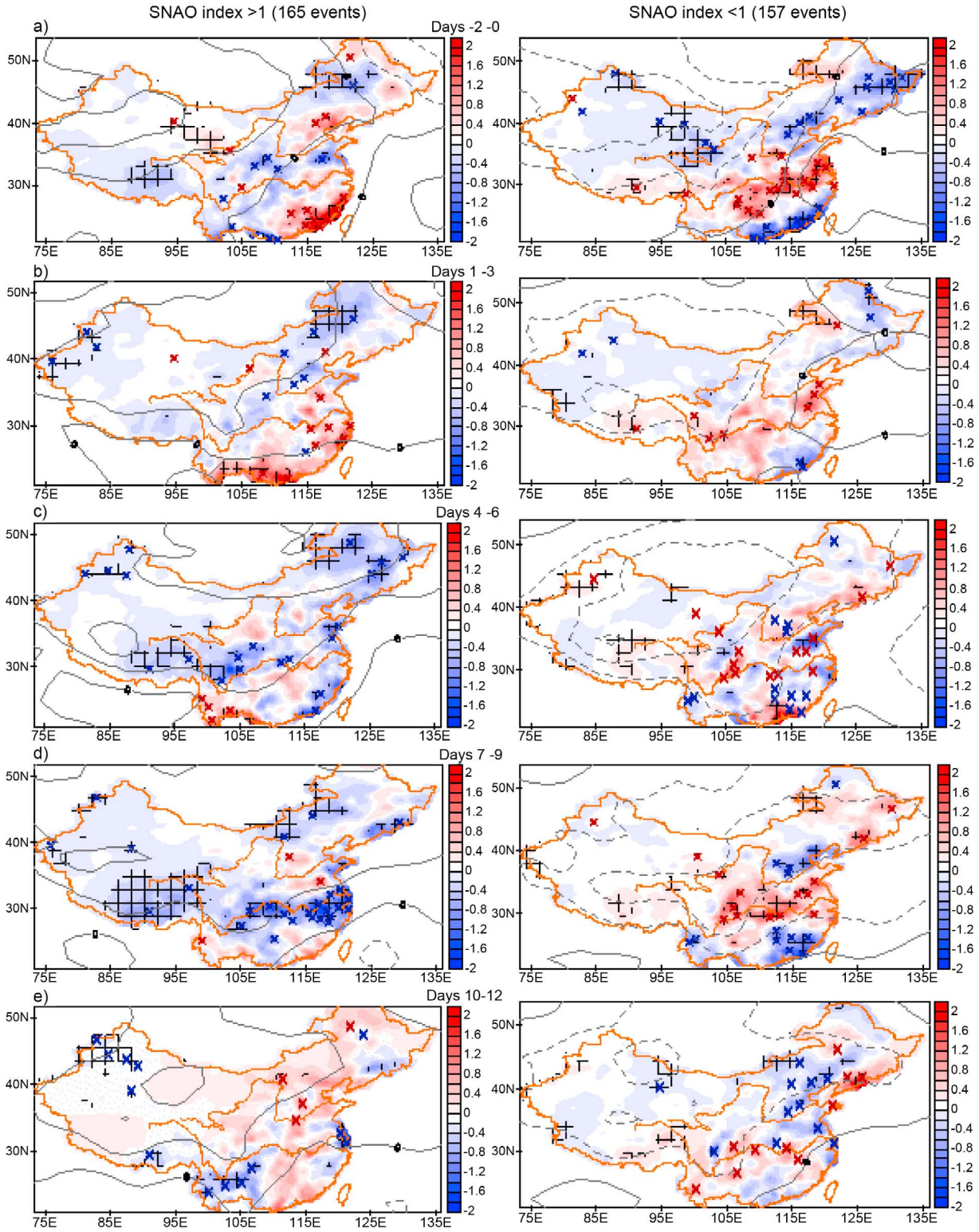

Figure 10. Same as Figure 8 but for daily precipitation anomalies (units: mm/d) in China from a gridded daily temperature data set [*Chen et al.*, 2010] and 160 stations with MSLP anomalies included (contour in 0.5, units: hPa). Grid points and stations with significant composite precipitation anomaly (5% level) are indicated by pluses (grid points) and red/blue crosses (station data).

160 stations. It is clear that opposite precipitation anomaly patterns are found during positive and negative SNAO events, and the strongest signals are found around a week after the initiation of SNAO events, corresponding to the findings in Figure 9. During the development of positive SNAO events, positive precipitation anomalies are found in southeastern China as well as small regions in the northeast and central China, and negative precipitation anomalies are found in northeastern and southwestern (including the Tibetan Plateau) China. After three days, the negative precipitation anomalies in northeastern China become more pronounced as the positive MSLP anomaly (Figure 8) moves to the east, while the positive anomalies in southern China and the negative anomalies in the southwest weaken. After 4–6 days of positive SNAO events, the negative precipitation anomaly in northeast China is strengthened and a clear negative precipitation anomaly is found situated between the Yangtze River and Yellow River basins. This is consistent with positive MSLP anomalies in this region (Figure 8). The negative precipitation anomalies move eastward and southeast 7–9 days after positive SNAO events, consistent with the movement of the MSLP anomaly. During the development of negative SNAO events, negative precipitation anomalies are found in southeast and northeast China, with positive precipitation anomalies in the Yangtze River basin. The negative precipitation anomaly over northeast China then disappears and a positive precipitation anomaly appears over the Yellow River, Huai River and the upper to middle reaches of Yangtze River after 1–3 and 4–6 days, again consistent with the negative MSLP anomaly moving eastward. The positive precipitation anomaly over northeast China moves east after 4–6 days and there is a strengthening of the positive precipitation anomalies in south central China after 7–9 days, after which the signal weakens.

5. Conclusion

[27] Previous work on linking NAO and AO variability with climate in China have mainly shown lagged responses of summer climate to the winter or spring NAO and AO, thus suggesting an indirect effect of these modes. We have shown here, however, that summer, July–August, NAO (SNAO) variability is almost concurrent with a substantial component of the summer climate variability in China. A maximum influence occurs on precipitation when the SNAO leads by about a week or slightly more, with a similar effect on MSLP. Despite this lag for maximum influence, there is a strong concurrent relationship as well. Our results suggest that this teleconnection between the North Atlantic region and the East Asian Monsoon, particularly evident over China, arises from (1) near simultaneous responses of the atmospheric circulation in East Asia and the positive/negative phases of the SNAO, where both are part of large-scale midlatitude to high-latitude atmospheric circulation teleconnections in the summer Northern Hemisphere, and (2) propagation of the SNAO signal to eastern China in about one week after the maximum of a positive or negative SNAO event. The results are encouraging for better understanding extratropical influences on summer East Asian climate, especially the EASM, and may provide useful guidance for improving the detailed performance of seasonal climate models and thus seasonal forecasting of East Asian, particularly Chinese, summer climate. Because of the hemispheric nature of these teleconnections, there are implications for climate models generally. These interannual teleconnections, and decadal teleconnections, will be further investigated through ensembles of atmospheric and coupled model ensemble runs representing the last century or so. The new availability of 6 hourly tropospheric reanalysis data over the last 140 years [*Compo et al.*, 2011] may allow decadal as well as interannual mechanisms to be further studied with the help of such integrations, taking account of additional forcing factors such as ENSO and climate warming.

[28] **Acknowledgments.** This work was partly supported by Swedish International Development Cooperation Agency SIDA (project SWE-2009-245) and the Swedish Research Council. Chris Folland was supported by the Joint DECC/Defra Met Office Hadley Centre Climate Programme (GA01101) Daoyi Gong was supported by 2008AA121704. The paper contributes to the CLIVAR International Climate of the Twentieth Century project (http://www.iges.org/c20c/) and the Swedish strategic research area Modeling the Regional and Global Earth system, MERGE. This is contribution 5 from the Sino-Swedish Centre for Tree ring Research (SISTRR).

References

Ansell, T. J., et al. (2006), Daily mean sea level pressure reconstructions for the European-North Atlantic region for the period 1850–2003, *J. Clim.*, *19*(12), 2717–2742, doi:10.1175/JCLI3775.1.

Barnston, A. G., and R. E. Livezey (1987), Classification, seasonality and persistence of low-frequency atmospheric circulation patterns, *Mon. Weather Rev.*, *115*, 1083–1126, doi:10.1175/1520-0493(1987)115<1083:CSAPOL>2.0.CO;2.

Beck, C., J. Grieser, and B. Rudolf (2005), A new monthly precipitation climatology for the global land areas for the period 1951 to 2000, in Klimastatusbericht KSB 2004, report, pp. 181–190, DWD, Offenbach, Germany (Available at http://dwd.de.)

Branstator, G. (2002), Circumglobal teleconnections, the jet stream waveguide, and the North Atlantic Oscillation, *J. Clim.*, *15*(14), 1893–1910, doi:10.1175/1520-0442(2002)015<1893:CTTJSW>2.0.CO;2.

Chang, C. P., Y. S. Zhang, and T. Li (2000), Interannual and interdecadal variations of the East Asian summer monsoon and tropical Pacific SSTs. Part I: Roles of the subtropical ridge, *J. Clim.*, *13*(24), 4310–4325, doi:10.1175/1520-0442(2000)013<4310:IAIVOT>2.0.CO;2.

Chang, C. P., K. M. Lau, and H. Hendon (2006), The Asian winter monsoon, in *The Asian Monsoon*, edited by B. Wang, pp. 89–127, Springer, New York, doi:10.1007/3-540-37722-0_3.

Chen, D., T. Ou, L. Gong, C. Y. Xu, W. Li, C.-H. Ho, and W. Qian (2010), Spatial interpolation of daily precipitation in China: 1951–2005, *Adv. Atmos. Sci.*, *27*, 1221–1232, doi:10.1007/s00376-010-9151-y.

Compo, G. P., et al. (2011), The Twentieth Century Reanalysis Project, *Q. J. R. Meteorol. Soc.*, *137*(654), 1–28, doi:10.1002/qj.776.

Ding, Y. (2004), Seasonal March of the East-Asian Summer Monsoon, in *East Asian Monsoon*, *World Sci. Ser. Meteorol. East Asia*, vol. 2, edited by C.-P. Chang, pp. 3–53, World Sci., Hackensack, N. J.

Ding, Y., and J. C. L. Chan (2005), The East Asian summer monsoon: An overview, *Meteorol. Atmos. Phys.*, *89*(1–4), 117–142, doi:10.1007/s00703-005-0125-z.

Ding, Y. H., and G. Q. Hu (2003), A study on water vapor budget over China during the 1998 severe flood periods, *Acta Meteorol. Sin.*, *61*(2), 129–145.

Ding, Y., Z. Wang, and W. Sun (2008), Inter-decadal variation of the summer precipitation in East China and its association with decreasing Asian summer monsoon. Part I: Observed evidences, *Int. J. Climatol.*, *28*(9), 1139–1161, doi:10.1002/joc.1615.

Feng, S., and Q. Hu (2008), How the North Atlantic Multidecadal Oscillation may have influenced the Indian summer monsoon during the past two millennia?, *Geophys. Res. Lett.*, *35*, L01707, doi:10.1029/2007GL032484.

Folland, C. K., J. Knight, H. W. Linderholm, D. Fereday, S. Ineson, and J. W. Hurrell (2009), The summer North Atlantic Oscillation: Past, present, and future, *J. Clim.*, *22*(5), 1082–1103, doi:10.1175/2008JCLI2459.1.

Gemmer, M., S. Becker, and T. Jiang (2004), Observed monthly precipitation trends in China 1951–2002, *Theor. Appl. Climatol.*, *77*, 39–45, doi:10.1007/s00704-003-0018-3.

Gong, D., and Z. He (2002), Interdecadal change in western Pacific subtropical high and climatic effects (in Chinese with English abstract), *Acta Geogr. Sin.*, *57*(2), 185–193.

Gong, D., and C.-H. Ho (2003), Arctic oscillation signals in the East Asian summer monsoon, *J. Geophys. Res.*, *108*(D2), 4066, doi:10.1029/2002JD002193.

Gong, D. Y., S. W. Wang, and J. H. Zhu (2001), East Asian winter monsoon and Arctic Oscillation, *Geophys. Res. Lett.*, *28*(10), 2073–2076, doi:10.1029/2000GL012311.

Gong, D., J. Zhu, and S. Wang (2002), Significant correlation between earlier Arctic oscillation and summer precipitation in Yangtze River (in Chinese), *Chin. Sci. Bull.*, *47*(7), 546–549.

Goswami, B. N., M. S. Madhusoodanan, C. P. Neema, and D. Sengupta (2006), A physical mechanism for North Atlantic SST influence on the Indian summer monsoon, *Geophys. Res. Lett.*, *33*, L02706, doi:10.1029/2005GL024803.

Gu, W., C. Li, W. Li, W. Zhou, and J. C. L. Chan (2009), Interdecadal unstationary relationship between NAO and east China's summer precipitation patterns, *Geophys. Res. Lett.*, *36*, L13702, doi:10.1029/2009GL038843.

Hong, C.-C., H.-H. Hsu, H.-H. Chia, and C.-Y. Wu (2008), Decadal relationship between the North Atlantic Oscillation and cold surge frequency in Taiwan, *Geophys. Res. Lett.*, *35*, L24707, doi:10.1029/2008GL034766.

Hung, C. W., X. Liu, and M. Yanai (2004), Symmetry and asymmetry of the Asian and Australian summer monsoons, *J. Clim.*, *17*(12), 2413–2426, doi:10.1175/1520-0442(2004)017<2413:SAAOTA>2.0.CO;2.

Hurrell, J. W., and C. K. Folland (2002), The relationship between tropical Atlantic rainfall and the summer circulation over the North Atlantic, *CLIVAR Exchanges*, *25*, 52–54.

Hurrell, J. W., and H. van Loon (1997), Decadal variations in climate associated with the North Atlantic Oscillation, *Clim. Change*, *36*, 301–326, doi:10.1023/A:1005314315270.

Hurrell, J. W., Y. Kushnir, G. Ottersen, and M. Visbeck (2003), An overview of the North Atlantic Oscillation, in *The North Atlantic Oscillation: Climatic Significance and Environmental Impact*, *Geophys. Monogr. Ser.*, vol. 134, edited by J. W. Hurrell et al., pp. 1–35, AGU, Washington, D. C.

Kistler, R., et al. (2001), The NCEP-NCAR 50 year reanalysis: Monthly means CD-ROM and documentation, *Bull. Am. Meteorol. Soc.*, *82*(2), 247–267, doi:10.1175/1520-0477(2001)082<0247:TNNYRM>2.3.CO;2.

Lau, K.-M., K.-M. Kim, and S. Yang (2000), Dynamical and boundary forcing characteristics of regional components of the Asian summer monsoon, *J. Clim.*, *13*(14), 2461–2482, doi:10.1175/1520-0442(2000)013<2461:DABFCO>2.0.CO;2.

Li, H. M., A. G. Dai, T. J. Zhou, and J. Lu (2010), Responses of East Asian summer monsoon to historical SST and atmospheric forcing during 1950–2000, *Clim. Dyn.*, *34*(4), 501–514, doi:10.1007/s00382-008-0482-7.

Li, J., R. Yu, and T. Zhou (2008), Teleconnection between NAO and climate downstream of the Tibetan Plateau, *J. Clim.*, *21*(18), 4680–4690, doi:10.1175/2008JCLI2053.1.

Liu, X., and Z. Y. Yin (2001), Spatial and temporal variation of summer precipitation over the Eastern Tibetan Plateau and the North Atlantic Oscillation, *J. Clim.*, *14*(13), 2896–2909, doi:10.1175/1520-0442(2001)014<2896:SATVOS>2.0.CO;2.

Lu, A. (2009), Impacts of global warming on patterns of temperature change in China, *J. Mountain Sci.*, *6*, 405–410, doi:10.1007/s11629-009-0166-8.

Lu, R., B. Dong, and H. Ding (2006), Impact of the Atlantic Multidecadal Oscillation on the Asian summer monsoon, *Geophys. Res. Lett.*, *33*, L24701, doi:10.1029/2006GL027655.

Mitchell, T. D., and P. D. Jones (2005), An improved method of constructing a database of observations and associated high-resolution grids, *Int. J. Climatol.*, *25*(6), 693–712, doi:10.1002/joc.1181.

Ninomiya, K., and C. Kobayashi (1999), Precipitation and moisture balance of the Asian summer monsoon in 1991. Part II: Moisture transport and moisture balance, *J. Meteorol. Soc. Jpn.*, *77*, 77–99.

Plumb, R. A. (1985), On the three-dimensional propagation of stationary waves, *J. Atmos. Sci.*, *42*(3), 217–229, doi:10.1175/1520-0469(1985)042<0217:OTTDPO>2.0.CO;2.

Qian, Y., and F. Giorgi (1999), Interactive coupling of regional climate and sulfate aerosol models over East Asia, *J. Geophys. Res.*, *104*(D6), 6477–6499, doi:10.1029/98JD02347.

Qian, Y., C. Fu, R. Hu, and Z. Wang (1996), Effects of industrial SO_2 emission on temperature variation in China and East Asia (in Chinese), *Clim, Environ. Res.*, *2*, 143–149.

Ren, G., H. Wu, and Z. Chen (2000), Spatial patterns of change trend in rainfall of China (in Chinese with English abstract), *Q. J. Appl. Meteorol.*, *11*(3), 322–330.

Robock, A., M. Mu, K. Vinnikov, and D. Robinson (2003), Land surface conditions over Eurasia and Indian summer monsoon rainfall, *J. Geophys. Res.*, *108*(D4), 4131, doi:10.1029/2002JD002286.

Rudolf, B., and F. Rubel (2005), Global precipitation, in *Observed Global Climate: New Series on Landolt-Börnstein, Numerical Data and Functional Relationships*, edited by M. Hantel, pp. 11.1–11.24, Springer, Berlin.

Rudolf, B., and U. Schneider (2005), calculation of gridded precipitation data for the global land-surface using in-situ gauge observations, paper presented at 2nd Workshop of the International Precipitation Working Group, IPWG, Monterey, Calif.

Rudolf, B., H. Hauschild, W. Rueth, and U. Schneider (1994), Terrestrial precipitation analysis: Operational method and required density of point measurements, in *Global Precipitations and Climate Change*, *NATO ASI Ser. I*, vol. 26, edited by M. Desbois and F. Desalmond, pp. 173–186, Springer, New York.

Schneider, U., T. Fuchs, A. Meyer-Christoffer, and B. Rudolf (2008), Global precipitation analysis products of the GPCC, report, 12 pp., DWD, Offenbach, Germany. (Available at www.ksb.dwd.de)

Sha, W., and Q. Guo (1998), Variations of summer rainfall over China in relation to the geographical locality of subtropical high ridge over West Pacific (in Chinese with English abstract), *Q. J. Appl. Meteorol.*, *9*, supplement, 31–38.

Smith, T. M., R. W. Reynolds, T. C. Peterson, and J. Lawrimore (2008), Improvements to NOAA's historical merged land-ocean surface temperature analysis (1880–2006), *J. Clim.*, *21*(10), 2283–2296, doi:10.1175/2007JCLI2100.1.

Sun, J., H. Wang, and W. Yuan (2008), Decadal variations of the relationship between the summer North Atlantic Oscillation and middle East Asian air temperature, *J. Geophys. Res.*, *113*, D15107, doi:10.1029/2007JD009626.

Sung, M.-K., W.-T. Kwon, H.-J. Baek, K.-O. Boo, G.-H. Lim, and J.-S. Kug (2006), A possible impact of the North Atlantic Oscillation on the east Asian summer monsoon precipitation, *Geophys. Res. Lett.*, *33*, L21713, doi:10.1029/2006GL027253.

Sung, M.-K., G.-H. Lim, and J.-S. Kug (2010), Phase asymmetric downstream development of the North Atlantic Oscillation and its impact on the East Asian winter monsoon, *J. Geophys. Res.*, *115*, D09105, doi:10.1029/2009JD013153.

Takaya, K., and H. Nakamura (1997), A formulation of a wave-activity flux for stationary Rossby waves on a zonally varying basic flow, *Geophys. Res. Lett.*, *24*(23), 2985–2988, doi:10.1029/97GL03094.

Takaya, K., and H. Nakamura (2001), A formulation of a phase-independent wave-activity flux for stationary and migratory quasigeostrophic eddies on a zonally varying basic flow, *J. Atmos. Sci.*, *58*(6), 608–627, doi:10.1175/1520-0469(2001)058<0608:AFOAPI>2.0.CO;2.

Wang, B. (2006), *The Asian Monsoon*, 787 pp., Springer, New York.

Wang, B., and Z. Fan (1999), Choice of South Asian summer monsoon indices, *Bull. Am. Meteorol. Soc.*, *80*(4), 629–638, doi:10.1175/1520-0477(1999)080<0629:COSASM>2.0.CO;2.

Wang, B., R. Wu, and K.-K. Lau (2001), Interannual variability of the Asian summer monsoon: Contrasts between the Indian and the western North Pacific–East Asian monsoons, *J. Clim.*, *14*(20), 4073–4090, doi:10.1175/1520-0442(2001)014<4073:IVOTAS>2.0.CO;2.

Wang, B., Z. W. Wu, J. P. Li, J. Liu, C. P. Chang, Y. H. Ding, and G. X. Wu (2008), How to measure the strength of the East Asian summer monsoon, *J. Clim.*, *21*(17), 4449–4463, doi:10.1175/2008JCLI2183.1.

Wang, C., F. Kucharski, R. Barimalala, and A. Bracco (2009), Teleconnections of the tropical Atlantic to the tropical Indian and Pacific Oceans: A review of recent findings, *Meteorol. Z.*, *18*, 445–454, doi:10.1127/0941-2948/2009/0394.

Wang, J. X. L., and D. J. Gaffen (2001), Late twentieth century climatology and trends of surface humidity and temperature in China, *J. Clim.*, *14*(13), 2833–2845, doi:10.1175/1520-0442(2001)014<2833:LTCCAT>2.0.CO;2.

Wang, S., and D. Gong, (2000), Enhancement of the warming trend in China, *Geophys. Res. Lett.*, *27*(16), 2581–2584, doi:10.1029/1999GL010825.

Watanabe, M. (2004), Asian jet waveguide and a downstream extension of the North Atlantic Oscillation, *J. Clim.*, *17*(24), 4674–4691, doi:10.1175/JCLI-3228.1.

Webster, P. J., V. O. Magaña, T. N. Palmer, J. Shukla, R. A. Tomas, M. Yanai, and T. Yasunari (1998), Monsoons: Processes, predictability, and the prospects for prediction, *J. Geophys. Res.*, *103*(C7), 14,451–14,510, doi:10.1029/97JC02719.

Wen, X. Y., S. W. Wang, J. H. Zhu, and D. Viner (2006), An overview of China climate change over the 20th century using UK UEA/CRU high resolution grid data (in Chinese with English abstract), *Chin. J. Atmos. Sci.*, *30*(5), 896–904.

Weng, H. Y., K. M. Lau, and Y. K. Xue (1999), Multi-scale summer rainfall variability over China and its long-term link to global sea surface temperature variability, *J. Meteorol. Soc. Jpn.*, *77*, 845–857.

Wu, G., J. Chou, Y. Liu, Y. Zhang, and S. Sun (2003), Review and prospect of the study on the subtropical anticyclone (in Chinese with English abstract), *Chin. J. Atmos. Sci.*, *27*(4), 503–517.

Wu, R.-G., and B. Wang (2002), A contrast of the east Asian summer monsoon–ENSO relationship between 1962–77 and 1978–93, *J. Clim.*, *15*(22), 3266–3279, doi:10.1175/1520-0442(2002)015<3266:ACOTEA>2.0.CO;2.

Xue, Y., T. M. Smith, and R. W. Reynolds (2003), Interdecadal changes of 30-yr SST normals during 1871–2000, *J. Clim.*, *16*(10), 1601–1612, doi:10.1175/1520-0442-16.10.1601.

Yang, S., and K.-M. Lau (1998), Influences of sea surface temperature and ground wetness on Asian summer monsoon, *J. Clim.*, *11*(12), 3230–3246, doi:10.1175/1520-0442(1998)011<3230:IOSSTA>2.0.CO;2.

Yang, S., K.-M. Lau, S.-H. Yoo, J. L. Kinter, K. Miyakoda, and C.-H. Ho (2004), Upstream subtropical signals preceding the Asian summer monsoon circulation, *J. Clim.*, *17*(21), 4213–4229, doi:10.1175/JCLI3192.1.

Zhang, Q., C. Xu, Z. Zhang, Y. Chen, and C. Liu (2009), Spatial and temporal variability of precipitation over China, 1951–2005, *Theor. Appl. Climatol.*, *95*, 53–68, doi:10.1007/s00704-007-0375-4.

Zhou, T., and R. Yu (2005), Atmospheric water vapour transport associated with typical anomalous summer rainfall patterns in China, *J. Geophys. Res.*, *110*, D08104, doi:10.1029/2004JD005413.

Zhou, T., et al. (2009), The CLIVAR C20C Project: Which components of the Asian-Australian Monsoon variability are forced and reproducible?, *Clim. Dyn.*, *33*(7–8), 1051–1068, doi:10.1007/s00382-008-0501-8.

D. Chen, J.-H. Jeong, H. W. Linderholm, and T. Ou, Regional Climate Group, Department of Earth Sciences, University of Gothenburg, SE-40530 Gothenburg, Sweden. (hansl@gvc.gu.se)

C. K. Folland, Met Office Hadley Centre for Climate Change, Exeter EX1 3PB, UK.

D. Gong, State Key Laboratory of Earth Surface Processes and Resource Ecology, Beijing Normal University, Beijing 100875, China.

H. Liu, Laboratory for Climate Studies, National Climate Center, China Meteorological Administration, 46 Zhongguancun Nandajie, Beijing 100081, China.

Y. Liu, State Key Laboratory of Loess and Quaternary Geology, Institute of Earth Environment, Chinese Academy of Sciences, 10 Fenghui South Road High-Tech Zone, Xi'an 710075, China.